JAAS

Exploration of LIBS as a novel and rapid elemental mapping technique of nuclear fuels in the form of surrogate TRISO particles

Journal:	*Journal of Analytical Atomic Spectrometry*
Manuscript ID	JA-ART-01-2023-000034.R2
Article Type:	Paper
Date Submitted by the Author:	08-May-2023

Complete List of Authors:	Manard, Benjamin; Oak Ridge National Laboratory, Chemical Science Division Andrews, Hunter; Oak Ridge National Laboratory, Radioisotope Science and Technology Division; Quarles Jr., C.; Elemental Scientific Inc, Bradley, Veronica; Oak Ridge National Laboratory Physical Sciences Directorate, Doyle, Peter; Oak Ridge National Laboratory, Nuclear Energy and Fuel Cycle Division Zirakparvar, N.; Oak Ridge National Laboratory Physical Sciences Directorate, Dunlap, Daniel; Oak Ridge National Laboratory Physical Sciences Directorate, Hexel, Cole; Oak Ridge National Laboratory, Nuclear Analytical Chemistry and Isotopi

Exploration of LIBS as a novel and rapid elemental mapping technique of nuclear fuels in the form of surrogate TRISO particles

Benjamin T. Manard[1*], Hunter B. Andrews[2*], C. Derrick Quarles Jr.[3], Veronica C. Bradley[1], Peter Doyle[4], N. Alex. Zirakparvar[1], Daniel. R. Dunlap[1], and Cole. R. Hexel[1]

1. Chemical Sciences Division, Oak Ridge National Laboratory, USA
2. Radioisotope Science and Technology Division, Oak Ridge National Laboratory, USA
3. Elemental Scientific Inc, USA
4. Nuclear Energy and Fuel Cycle Division, Oak Ridge National Laboratory, USA

[*]Corresponding Authors: B.T. Manard, manardbt@ornl.gov; H.B. Andrews, andrewshb@ornl.gov

Manuscript to be submitted to *Journal of Analytical Atomic Spectrometry*

Table of contents entry:

Depiction of the analysis of a surrogate tri-structural isotropic (TRISO) particle via laser-induced breakdown spectroscopy (LIBS)

Abstract

Laser-induced breakdown spectroscopy (LIBS) was employed to characterize coatings on surrogate fuel particles. Tri-structural isotropic (TRISO) particles are a proposed nuclear fuel alternative for high temperature reactors. These particles are constructed of a ZrO_2 kernel (as a surrogate to uranium), surrounded by an inner pyrolytic carbon layer and are surrounded by an outer carbide layer (ZrC, presented here) to act as a barrier to fission products generated during nuclear reactions. These particles are embedded within a graphite compact and housed within the reactor core. Simply put, due to their robust nature, performing elemental analysis of these particles poses a challenge. Presented here, LIBS is explored as a method for characterizing elemental constituents of these particles, with the focus being on rapid elemental mapping and depth profiling. Different from traditional elemental analysis techniques (e.g., inductively coupled plasma – based methods), LIBS is advantageous because it can directly analyze the sample surface and can detect light elements such as C and O, making it a viable technique for the analysis of small, multilayered particles as spatial elemental information is warranted in the production of these particles. In the work presented here, LIBS was successfully used for discerning small layers (30-50 μm), detecting the location of carbon and oxygen layers, providing fast 2-D mapping (<5 min particle^{-1}) and rapid depth profiling (10 s particle^{-1}).

Keywords: laser-induced breakdown spectroscopy, TRISO particles, LIBS imaging, elemental mapping, depth profiling, nuclear

Introduction

Laser-induced breakdown spectroscopy (LIBS) is a unique approach to performing elemental analysis of solid materials. In LIBS analysis, a short-pulsed (e.g., nanosecond (ns)) laser is focused onto the sample surface. In this pulse, a microplasma is formed on the sample surface in which a small amount (fg-ng's) of material is vaporized and ultimately excited and/or ionized within the plasma. The emitted photons from the plasma can be collected via optics and delivered to a spectrometer for measurement. Compared to traditional elemental analyses, LIBS offers many unique advantages such as little-to-no sample preparation, can provide spatial elemental measurements, and can detect light elements (e.g., H, C, O, F, etc.). While solution-based inductively coupled plasma – optical emission spectroscopy / mass spectrometry (ICP-OES/MS) is considered the primary choice for performing elemental analysis, it is ultimately not capable of analyzing light elements such as those mentioned above due to atmospheric plasma conditions (e.g., H, O, N) or lack of ionization potential to excite/ionize the element (e.g., F). When coupled with a translational stage, LIBS can be used to provide elemental imaging of samples.[1-3]

LIBS has become a widely used technique for a variety of samples and elemental determinations.[1, 4] More recently, LIBS has shown utility in the field of nuclear analytical chemistry where handheld (HH)-LIBS has been demonstrated for measuring both bulk and impurity levels in nuclear matrices[5-8], LIBS has been developed for real-time monitoring off-gasses and material interactions applicable to molten salt reactors[9-13], and LIBS tools for measuring uranium hexafluoride enrichment have been developed.[14-16] Ultimately, LIBS offers many advantages for the nuclear industry mainly due to its ability to perform analysis from a distance, or at the sample in a handheld configuration, making the technique very beneficial for working in radiological environments (e.g., glove boxes, reactors, etc.).

Another logical application of LIBS in the field of nuclear analytical chemistry is the analysis and characterization of tri-structural isotropic (TRISO) particles.[17] TRISO particles are a proposed advanced nuclear fuel form for use with high-temperature gas cooled reactors or liquid sodium cooled reactors. From the core working outwards the TRISO particles layers include a fuel kernel at the core (e.g., UO_2 or UCO), followed by a porous carbon layer, an inner pyrolytic carbon layer (PyC), a silicon carbide layer, and an additional outer PyC layer.[17] Thousands of these individual TRISO particles would be suspended into a graphite matrix to form a single fuel 'pebble'. This fuel form offers benefits over traditional nuclear fuel in terms of fission product retention and the resistance to becoming damaged in an accidental / unwanted scenario. Due to the robust and resistant design of these fuel forms, traditional analytical measurements such as bulk digestion ICP-MS/OES is difficult. Laser ablation–ICP-MS/OES would be a potential approach for elemental / isotopic mapping, however, light elements that make up a significant portion of the sample matrix (oxides, carbides, and carbon layers) would not be able to be adequately measured. Other techniques including scanning electron microscopy (SEM), energy dispersive x-ray spectroscopy (EDS), Raman scattering, x-ray diffraction (XRD), and x-ray imaging have previously been utilized.[18, 19] Liu et al. demonstrated the use of these methodologies when investigating improved methods of chemical vapor deposition (CVD); however, Raman and XRD were only used on specific layers to investigate the CVD process, only a single SEM-EDS map is shown with no mention of measurement time, and the only large volume measurement was the overall particle diameter.[18] Here, LIBS provides an alternative analytical approach that is feasible for light and heavy elements allowing all layers to be interrogated and can be performed rapidly to enable better insight into TRISO particle production or analysis of particle performance after being irradiated in a reactor. For example, LIBS elemental mapping may offer an alternative to

SEM-EDS mapping at a fraction of the measurement time permitting large sample sizes to be evaluated. Previously, Roberts et al. utilized femtosecond-LIBS to investigate silver transport in surrogate TRISO particles using depth profiling, but advances in LIBS methods in the past decade offer the opportunity for further levels of analysis.[20]

Presented here is the first demonstration of LIBS elemental mapping and depth profiling of ZrC/PyC/ZrO_2 layered particles (as surrogate for true TRISO particles), as well as examples of how LIBS could be employed for quality control during production to evaluate layer thicknesses and composition. This is critical as the different layers serve to contain fission products and protect the interior of the particle from interactions with the coolant fluid, too small a layer could result in fuel particle failure. These methodologies would also be relevant for post irradiation examination after these particles have been tested to evaluate the location and containment of fission product elements within the fuel. This work highlights the advantages of LIBS analysis including high spatial resolution, rapid measurements, and the ability to detect light and heavy elements simultaneously.

Experimental

Sample preparation

Fabrication of the ZrC-coated particles in this work was accomplished at Oak Ridge National Laboratory with a fluidized bed chemical vapor deposition system modified for delivery of a $ZrCl_4$ precursor. The details of the system can be found in other work.[21, 22] The Deep Burn (DB)-ZrC-44 sample substrates consisted of yttria stabilized zirconia kernels (nominally 525 μm diameter) coated with 50 μm of PyC. ZrC has been proposed as an additional TRISO layer or as a substitution for the typical SiC layer.[17] ZrC was deposited onto the outside of the PyC layer using $ZrCl_4$ and

CH_4 precursors with H_2 as a reaction gas and Ar as a carrier gas for the $ZrCl_4$ vapor and as the primary fluidization medium. The deposition chamber was held at 1500 °C and gas concentrations were maintained at 0.004 sccm CH_4 per total gas sccm and 0.007 sccm Cl_2 per total gas sccm during the depositions. Characterization in that work showed a coating that was nearly stoichiometric and well-adhered to the underlying PyC. Additionally, several tools showed both a ZrC matrix and nanocrystalline or amorphous carbon deposits throughout the coating. These deposits were found to be due to a more rapid deposition conditions than in more homogenous coatings developed through the coating effort. While this specific sample does not represent the highest quality ZrC coating produced through the DB program, it is an interesting specimen in the present work due it thickness (approximately 30 μm) and the carbon deposits. Furthermore, the complex deposition methodology lends itself to needing a high-throughput characterization method for quality control.

A photograph was taken of a sample surrogate TRISO particle (**Figure 1a**) with an Axiocam 712 (12MP camera) using the EC EPN 5x objective lens on a Zeiss Axioscope 5 microscope. The particle was adhered to a gunshot residue (GSR) tab and imaged perpendicular and at approximately 50°. Low magnification was used to allow for the greatest depth of focus. Images were taken with brightfield which has the illumination along the same axis as the imaging, The GSR-mounted particles were used for depth profile analysis.

The particles were also mounted in Buehler EpoThin 2 epoxy resin. Upon curing of the resin, the mount was ground down to expose the particles' cross-sections (approximately through their centers). The exposed particles were then polished down to 1 μm utilizing a combination of tungsten carbide and diamond abrasives. The finished mount was then cleaned using a commercial

detergent solution prior to analysis. The cross-sectioned particles were used for elemental mapping.

Scanning electron microscopy / energy dispersive X-ray Spectroscopy

Images were made using a thermionic-emission electron gun scanning electron microscope (SEM; Hitachi SU3800, Tokyo, Japan). Backscatter electron (BSE) micrographs were taken of the cross-section of surrogate TRISO particles mounted in a conductive epoxy. The analysis was conducted at 15 kV in high vacuum with magnification of 110 to 150×. This image can be seen in **Figure 1b**. The SEM was coupled with an EDAX Octane Elect Super energy dispersive X-ray spectrometer (EDS; Mahwah, New Jersey, USA). Characteristic X-rays were generated by the SEM electron beam and detected by a silicon drift detector. Line scans and EDS maps were collected to approximate elemental composition of the particles. Elemental concentrations were detectable at low percent levels. Line scans were analyzed with a dwell time of 20 ms, a line width of 10 μm, and a frame number of 68. The elemental area map had a dwell time of 200 μs and a frame number of 3851.

Laser-induced breakdown spectroscopy

An Elemental Scientific Lasers (Bozeman, MT, USA) imageGEO^{LIBS} equipped with an ESLumen spectrometer was employed for the high-speed LIBS elemental imaging of the samples. The LIBS measurement system is graphically represented in **Figure 2**. This integrated system is equipped with a 193 nm excimer laser which is focused within an XYR beam aperture (to generate square spots) into a helium (ultrahigh purity, 99.994%, Airgas, Radnor, PA, USA)-purged (1000 mL min^{-1}) TwoVol3 ablation chamber.[23] **Figure 2** shows the two sampling approaches used in this work:

a) a cross-sectioned surrogate TRISO particle mounted in epoxy for elemental mapping or b) a complete surrogate TRISO particle on a sticky tab for depth profiling. The typical LIBS analysis performed in this study utilized 100% laser energy which resulted in a beam energy density at the sample surface of 8.35 J cm^{-2} with a repetition rate of 200 Hz. This is a high repetition rate for a commercial system compared to those typically reported in ns-LIBS imaging studies.[1] For LIBS analysis, the emitted light from the laser-induced plasma was collected through a fiber sealed within the TwoVol3 analytical cup as shown in **Figure 2**. The light distributed into a 5-channel (encompassing 188-1099 nm), fixed grating (0.06-0.32 nm spectral resolution), Czerny-Turner spectrometer. For the experiments presented here, a spectrometer delay and integration of 0.3 μs and 3 ms was employed, respectively. All LIBS spectra were processed through iolite 4.8 software (Elemental Scientific Lasers)[23-25]. This processing includes the integration of the respective peaks including background subtraction for each of the emission peaks.

Results and Discussion

Investigation of the elemental composition of surrogate TRISO particles via LIBS

Initially, the various regions of the cross-section of a particle were analyzed via LIBS to determine its elemental composition. As previously mentioned, these particles consisted of three unique layers such that the core (kernel) consisted of yttria-stabilized ZrO_2 which is engulfed within a pyrolytic carbon (PyC) inner layer, and finally a ZrC shell. For verification of these elemental components, emission spectra were collected at each location, and representative spectra can be seen in **Figure 3**. Here, the spectra are segmented and presented within 3 regions (240-255, 480-495, and 770-800 nm) for simplicity. After inspection of the first segment (240-255 nm, **Figure**

3a) the C I 247 nm emission line is clearly present within the PyC inner layer with a small portion in the ZrC outer layer. Zr emission lines are found within the ZrC outer layer, and the ZrO_2 core, as expected. Additionally, the Y II 241 nm line is clearly seen in the core spectra and not in the outer ZrC layer. Inspection of the second segment (480-495 nm, **Figure 3b**) shows the same trend of Zr in the outer and core layer, and the Y II 490 nm line only in the core layer. Lastly, the third segment (770-800 nm, **Figure 3c**) details the detection of the O I 777 nm emission within the core. This of course is expected as the core is yttria stabilized zirconia.

LIBS mapping of surrogate TRISO particles

Next, 2-dimensional (2D) mapping was performed on cross-sectioned particles, prepared as described above. For these studies, 25 and 50 μm square laser spot sizes were employed with a scan speed was 1000 μm s^{-1} and 2000 μm s^{-1}, respectively, and a repetition rate of 200 Hz. The total time to map a particle was 5 min 16 s for the 25 μm square and 4 min 48 s for the 50 μm square. These spot size and scan speeds resulted in an 80% overlap between sequential shots resulting in an enhanced spatial resolution. The benefit of using overlapping spots, or oversampling, has been previously demonstrated.[23, 26, 27]

The resulting maps are presented in **Figure 4**. The outer ZrC layer of the surrogate TRISO particles was reported to be approximately 30 μm on average and it is clearly seen that the 25 μm square spot provides superior spatial resolution compared to the 50 μm square spot; indicating that the spot size needs to be on a similar scale to the feature dimensions. For comparison, and alternative version of the figure with SEM-EDS images is provided in the Supplementary Information (**Figure S1**).

In addition to scanning a single particle, a large area was mapped that encompasses 12 particles. This data is presented in **Figure 5**. Here, a 50 μm square spot was used, with an 80% overlap in the x and y directions (10 μm of new material ablated). This pattern was set up to raster at 2,000 μm s^{-1} and 200 Hz repetition rate. To map this area (5.66 × 4.25 mm) 426 lines were utilized, and the total time was 32 min 22 s. The figure shows that the particles have visibly reproducible features for the three layers of interest. Another map was made with a 25 μm square spot, with an 80% overlap in the x and y directions (5 μm of new material ablated). Here 1,000 μm s^{-1} scan speed was used with 200 Hz repetition rate, and the total time was 32 min 22 s (albeit a smaller area of 2.95 × 2.33 mm). The 25 μm square spots lead to higher resolution maps; however, it takes longer to analyze the same region as the 50 μm square spot. If LIBS mapping was used in post irradiation examination, a finer resolution to investigate fission product distribution would likely be desired. As seen in the 25 μm square spot map of **Figure 5**, the defects in the outer ZrC layer are far better resolved and the Y distribution in the kernel can be discerned as well.

Analysis of surrogate TRISO particles via line scan extractions

A unique feature of iolite 4.8 allows for the extraction of line scans from collected and processed LIBS (and LA-ICP-MS) data. While it is not uncommon to be able to extract a single line scan as performed, iolite allows the user to extract line scans along a user defined path across the ablation pattern. Meaning that while a 2D image is generated from left to right ablation lines, a selection can be made to view the data in any line across the 2D map (e.g., diagonally, or vertically).

Here, for three of the particles mapped within the 25 μm square spot pattern (**Figure 5**) 4 slices of each map were extracted (0º, 45º, 90º, and 135º rotated about the center). An SEM-EDS line scan

of a particle was analyzed and presented in **Figure 6a**. The collected slices were centered based on the ZrO_2 region intensities. For each surrogate TRISO particle these line scans were averaged and plotted in **Figure 6(b-d)**. While this SEM-EDS line scan does have higher resolution between the layers, it took ~150 min to generate a single data profile, meanwhile the LIBS mapping can analyze several particles and provide several line scans for each particle in ~30 min (presented here). Additionally, the SEM-EDS was unable to successfully detect Y, due to is interference with Zr, resulting in a false detection of Y in the ZrC layer. The benefit of the LIBS multitude of spectral emissions is highlighted here as convoluted peaks can be avoided simply by using alternate peaks. From the averaged line scans shown in **Figure 6** the kernel and two additional layers can be seen. A representative, unaveraged data set of line scans can be seen in the Supplementary Information (**Figure S2**). Additionally, the SEM-EDS profile layer transitions are projected onto the LIBS profiles as dashed lines. This was used as an aid to determine how the LIBS profile features may be evaluated to determine layer thicknesses despite the gradual transitions due to overlapping shots. It is apparent that the ZrC/PyC and the PyC/ZrO_2 interfaces align with the local maximum Zr and C intensities in the LIBS profiles, respectively. This is predicted as the maximum intensity would correlate to the last position prior to transitioning to the next layer (as the signal would then begin to decrease). The outer edge of the particles aligns at where the Zr intensities reach the background levels in both the SEM-EDS and LIBS profiles. Using the Zr and C peak intensity locations and the point where the Zr levels surpassed the background ($I_{Zr} > 3\sigma_{background}$), the layer thicknesses and core diameters were measured. The LIBS measurements are compared to those from the SEM-EDS line scans in **Table 1**. The values match well, and future measurements could use more slices from the 2D LIBS maps to decrease the uncertainty in each measurement. It is interesting to note that the %RSD is the lowest on the core measurement (1.7%) in comparison to

the middle and outer layers (6.3 and 16.2%, respectively). This is likely due to the LIBS technique detecting artifacts within the production of such particles. Possibly, the cores of the particles are likely the most repeatable to produce and inherent challenges arise from the deposition of subsequent layers. A SEM image of an example defect of the outer layer is provided within the Supplementary Information (**Figure S3**). It is also worth noting these mounted particles are not at the true midplane so any measured diameters or thickness would be skewed by the concentric spherical geometry. Here, the surrogate particle kernels were the best resolved and were measured to be 433.3 ± 7.6 μm. This being less than the reported nominal diameter indicates the mounts were indeed offset from the midplane.

Table 1. Averaged layer thicknesses and kernel diameter determined from LIBS slices and SEM-EDS line scans.

	Thickness/Diameter (μm)		
	ZrC Layer	**PyC Layer**	**ZrO2 Kernel**
LIBS	35.8 ± 5.8	42.5 ± 2.7	433.3 ± 7.6
SEM-EDS	38.4 ± 2.3	44.5 ± 1.2	441.0

Values based on the average of n replicates: (LIBS: ZrC n=6, PyC n=6, Kernel n=3; SEM: ZrC n=2, PyC n=2).

LIBS depth profiling of surrogate TRISO particles

Depth profiling by LIBS can be a beneficial tool to determining elemental information in the z-direction as opposed to the traditional x-y (i.e., 2D) mapping.[28-30] Typically, higher resolution can also be achieved in this modality as the spatial resolution is achieved via laser coupling with the sample, thus ablating a small portion (~nm) in the z-direction, rather than spot size (~μm). Here, we investigated the utilization of high speed (200 Hz) LIBS depth profiling of the surrogate particles. In this study, the particles (10×) were placed onto a GSR tab and loaded into the ablation cell (**Figure 2b**). In each sample, the laser was focused onto the highest point of the particle and a

100 × 100 μm square ablation was utilized. Each sample was analyzed for 10 s at 200 Hz (2000 laser pulses). The collected data was then processed in iolite such that the C 247, Zr 414, O 777, and Y 490 nm emission lines were integrated for each laser pulse. The averaged and normalized elemental intensities versus shot number were plotted (**Figure 7a**). In addition to the elemental depth profiles, LIBS provides the unique ability to compare the levels of light elements and metals. For example, the ratios of O to Zr and Zr to C are shown versus shot number in **Figure 7b and 7c**, respectively. Here it can be seen that the Zr to C ratio remains constant in the outer ZrC layer and the ratio asymptotes when the ZrO_2 kernel is reached. The O to Zr ratio offers an interesting insight that there is a minor inhomogeneity in the ZrO_2 kernel where O appears to be more concentrated further into the core. This could be due to the heating processes (1500 °C) in the production of the surrogate particles. Pisonero et al. had seen similar results when using glow discharge (GD) – sector field mass spectrometry (SFMS) for the analysis of heat-treated coatings.[31]

The slow decay of the Zr moving into the PyC layer and the slow decay of the C moving into the ZrO_2 kernel is likely due to re-depositing of the ablated material from the previous shots / sampling of the laser crater side wall. This 'smearing' between layers has been seen in other LIBS depth profiling work.[28] Mateo et al. utilized an alternative method to examining the elemental intensity depth profiles by investigating the linear correlation coefficients between spectra to better distinguish layers and where the layer interfaces lie.[28] Using this method, Mateo et al. was able to reliably determine the layer thicknesses of ceramic and polymer coatings on steel. To perform this correlation analysis, all spectra were ratioed with one another to determine the Pearson correlations coefficients. The Pearson correlation coefficient (r) relates the covariance between two variables (spectra):

$$r = \frac{\sum(x_i - \bar{x})(y_j - \bar{y})}{\sqrt{\sum(x_i - \bar{x})^2 (y_j - \bar{y})^2}}, \quad (1)$$

where x_i and y_j are the individual spectra being compared to one another and $\bar{x}$ and $\bar{y}$ are the mean values of each i^{th} and j^{th} spectra, respectively. A Pearson correlation value of 1 indicates are perfect positive correlation, a value of -1 indicates a perfect negative correlation, and a value of 0 indicates no correlation between the spectra. Each of the 2000 spectra were iteratively used in Equation 1 to provide a 2D Pearson correlation plot (**Figure 8**), a heatmap containing 4 million Pearson correlation coefficient pixels (2000 spectra squared) that reveals regions of similarities along the depth profile. When looking along the diagonal of this 2D correlation plot three bright yellow regions can be seen, the corresponding shot numbers where these regions change (denoted with circle markers) indicate the interface between two layers.

This correlation analysis was repeated for each depth profile replicate to determine the average number of laser pulses per layer of the surrogate TRISO particles. These values were used along with the reported ZrC and PyC layer thicknesses to determine the ablation rates for each material under these testing conditions. The laser pulses per layer and corresponding ablation rates are provided in **Table 2**. Logically, the ablation rate of ZrC is far lower than that of the PyC as the ZrC layer has a far greater hardness. The repeatability of these ten measurements is highlighted with %RSD values of 5.7 and 7.1% for the ZrC and PyC layers, respectively.

Table 2. Ablation rate determined from depth profiles and correlation analysis.

	ZrC Layer	**PyC Layer**	**ZrO_2 Kernel**
Laser Pulses	1 → 387 ± 22	387 ± 22 → 703 ± 29	703 ± 29→
Ablation Rate (nm pulse^{-1})	77.6 ± 4.4	158.2 ± 11.2	n/a

Values based on the average of 10 replicates (n=10). Depth based on the reported 30 μm ZrC and 50 μm PyC layer thicknesses.

These ablation rates, or similarly produced values, could be used in future quality control testing during TRISO production where random subsamples routinely undergo depth profiling to ensure

adequate layer thicknesses are being produced. While these results are preliminary, and further investigation is warranted, LIBS depth profiling could be a very useful approach for the high throughput analysis for TRISO particles production. The representative data (10 samples) was collected in ~100 s. When considering this as an option for quality control (QC) one could envision the ability to rapidly characterize 100 particles, for example, in <1 h. With higher laser frequencies and fewer shots (e.g., only 1000 shots to breach the ZrO_2 kernel) this would easily scale for production needs and providing key information on layer thickness, as well as the potential to detect impurities and defects.

Conclusions

The work presented here demonstrates a novel application of LIBS analysis, including elemental mapping and depth profiling, which could be applied to TRISO particles or other layered/coated particles. Here, high speed LIBS analysis was performed such that elemental analysis of surrogate TRISO particles was achieved for the detection of Zr, C, O, and Y. Ultimately this could provide a unique approach to the analysis of TRISO particles, as other analytical methods face issues related to the accident tolerant design of this fuel material. While the gold standard approach would be SEM / EDS, this approach is laborious, time consuming, and can result in false positives from overlapping peaks, which would not bode well for the analysis of hundreds / thousands of these particles. Here, depth profiling of a single particle could be achieved in <30 s, while 2D mapping of a single particle could be achieved in <5 min. This would be advantageous for quality control measurements during production to catch bad production lots. The methods shown in this study would also be useful for analyzing TRISO particles post-irradiation. The LIBS system could be configured in a glovebox- or hot cell-enclosed system. In this case LIBS could evaluate fission product yields to determine burnup and map fission product transport which would be especially

useful as these advanced fuels continue to be developed and tested. It should be noted that there are spatial resolution limitations for LIBS mapping and with limits of detection on the scale of 10-100's of parts-per-million LIBS may need to be coupled with laser ablation – ICP-MS for the optimal fission product mapping capabilities.

Acknowledgements

This work was supported by the Laboratory Directed Research and Development Program of Oak Ridge National Laboratory, managed by UT-Battelle, LLC, for the U.S. Department of Energy under contract DE-AC-05-000R22725. The authors would like to acknowledge Adam Malin (ORNL) for the assistance with graphics and Mark Boris (ORNL) for the assistance with optical images presented within this manuscript. Coating development was supported by the DOE Deep Burn Program and coating characterization was supported under NASA's Space Technology Mission Directorate (STMD) through the Space Nuclear Propulsion (SNP) project.

Figure Captions

Figure 1. Photograph of a surrogate tri-structural isotropic (TRISO) particle (a) and a scanning electron microscopy (SEM) image of its cross-section.

Figure 2. Depiction of the ImageGEO 193 LIBS experimental measurement system highlighting the novel LIBS TwoVol3 analytical cup with an embedded optical fiber to capture plasma emissions. The two sampling modes (a) elemental mapping and (b) depth profiling modes are shown in the cutaway graphics. For elemental mapping surrogate TRISO particle cross-sections mounted in epoxy were pulsed with a 200 Hz 193 nm laser as the translational stage was scanned side to side. For depth profiling, the stage was used to focus on the outer surface and then held constant as the laser bored into the sample. The LIBS system is enclosed in qualified laser glass (orange) to allow for operation as a class 1 embedded laser system.

Figure 3. LIBS spectra of three locations (core, inner layer, outer layer), within a surrogate TRISO particle segmented into three different regions: (a) 240-255, (b) 480-495, and (c) 770-800 nm.

Figure 4. LIBS mapping of a single surrogate TRISO particle using a 25 and 50 μm square spot, and its respective elemental distribution colored relative to the intensity color bar shown in the Y maps (purple-low, yellow-high). The far-right maps are shown in an RGB scale defined as green: O 777 nm, blue: Zr 414 nm, and red: C 247 nm. Colors which are mixtures of these fundamental colors visualize different compositions in the map. This is illustrated in the teal core representing a mixture of Zr and O, whereas the outer layer is a more pure blue due to the lack of O.

Figure 5. LIBS mapping of multiple surrogate TRISO particles with their respective elemental distributions at different laser spot sizes. Each element is mapped individually and is colored relative to intensity (purple-low, yellow-high).

Figure 6. Comparison of (a) SEM-EDS line scan and (b-d) averaged LIBS line scans of various surrogate TRISO particles. Each LIBS subplot (b-d) is the average of four cross-sectional slices taken from the elemental maps shown in Figure 5; the orientation of these slices along a surrogate TRISO particle is illustrated above the legend. The layer transitions seen in the SEM-EDS line scan are projected onto the LIBS plots to better understand features of the LIBS profiles.

Figure 7. Depth profiling of surrogate TRISO particles depicting an average of 10 replicates of (a) C, O, Zr, and Y normalized intensities, along with the average (b) O to Zr and (c) Zr to C ratios versus shot number.

Figure 8. 2D Pearson correlation plot where each depth profile spectra is compared to one another to visualize spatial correlations. The heatmap color represents the calculated Pearson correlation coefficient where a value of 1 indicates a perfect correlation. The diagonal of this plot (dashed line) was used to determine the transitions between the surrogate TRISO particle layers. The transitions are located where the colors changeover from yellow to purple, and vice versa, along this diagonal line (indicated by the circled points).

References

1. A. Limbeck, L. Brunnbauer, H. Lohninger, P. Pořízka, P. Modlitbová, J. Kaiser, P. Janovszky, A. Kéri and G. Galbács, *Anal. Chim. Acta*, 2021, **1147**, 72-98.
2. L. Jolivet, M. Leprince, S. Moncayo, L. Sorbier, C.-P. Lienemann and V. Motto-Ros, *Spectrochim. Acta, Part B*, 2019, **151**, 41-53.
3. V. Piñon, M. Mateo and G. Nicolas, *Appl. Spectrosc. Rev.*, 2013, **48**, 357-383.
4. R. S. Harmon and G. S. Senesi, *Appl. Geochem.*, 2021, **128**, 104929.
5. B. T. Manard, E. M. Wylie and S. P. Willson, *Appl. Spectrosc.*, 2018, **72**, 1653-1660.
6. A. P. Rao, P. R. Jenkins, J. D. Auxier, M. B. Shattan and A. K. Patnaik, *J. Anal. At. Spectrom.*, 2022, **37**, 1090-1098.
7. A. P. Rao, P. R. Jenkins, D. M. Vu, J. D. Auxier II, A. K. Patnaik and M. B. Shattan, *Analytical Methods*, 2021, **13**, 3368-3378.
8. H. B. Andrews, L. R. Sadergaski and K. G. Myhre, *Journal of Analytical Atomic Spectrometry*, 2022, **37**, 768-774.
9. H. B. Andrews, J. McFarlane and K. G. Myhre, *Applied Spectroscopy*, 2022, 00037028221088625.
10. H. B. Andrews, P. K. Thallapally and A. J. Robinson, *Micromachines*, 2023, **14**, 82.
11. H. B. Andrews and K. G. Myhre, *Applied Spectroscopy*, 2022, 00037028211070323.
12. K. G. Myhre, H. B. Andrews, D. Sulejmanovic, C. I. Contescu, J. R. Keiser and N. C. Gallego, *Journal of Analytical Atomic Spectrometry*, 2022, **37**, 1629-1641.
13. J. R. Keiser, P. M. Singh, M. J. Lance, H. M. M. Iii, K. G. Myhre, T. M. Lowe, D. Sulejmanovic, E. Cakmak, V. A. Cox, C. S. Hawkins and A. W. Willoughby, *J Nucl Mater*, 2022, **565**.
14. G. C. Chan, L. R. Martin and R. E. Russo, *Applied Spectroscopy*, 2022, 00037028221112953.
15. G. C.-Y. Chan, L. R. Martin, L. D. Trowbridge, Z. Zhu, X. Mao and R. E. Russo, *Spectrochim. Acta, Part B*, 2021, **176**, 106036.
16. K. M. Peruski, T. A. Davis, G. C.-Y. Chan, X. Mao, L. Trowbridge and L. R. Martin, *J. Fluorine Chem.*, 2022, **255**, 109951.
17. I. E. Porter, T. W. Knight, M. C. Dulude, E. Roberts and J. Hobbs, *Nucl Eng Des*, 2013, **259**, 180-186.
18. R. Liu, M. Liu, J. Chang, Y. Shao and B. Liu, *Journal of Nuclear Materials*, 2015, **467**, 917-926.
19. E. H. Kwapis, H. Liu and K. C. Hartig, *Progress in Nuclear Energy*, 2021, **140**, 103913.
20. D. Roberts, A. Du Plessis, J. Steyn, L. Botha, C. Strydom and I. Van Rooyen, *Spectrochimica Acta Part B: Atomic Spectroscopy*, 2010, **65**, 918-926.
21. J. D. H. James H. Miller, Brian C. Jolly, Paul A. Menchhofer, 2009.
22. J. H. M. Elliott S. Fray, Brian C. Jolly, John D. Hunn, 2011, **ORNL/TM-2010/295**.
23. B. T. Manard, C. J. Hintz, C. D. Quarles Jr, W. Burns, N. A. Zirakparvar, D. R. Dunlap, T. Beiswenger, A. M. Cruz-Uribe, J. A. Petrus and C. R. Hexel, *Metallomics*, 2022, **14**, mfac050.
24. C. Paton, J. Hellstrom, B. Paul, J. Woodhead and J. Hergt, *J. Anal. At. Spectrom.*, 2011, **26**, 2508-2518.
25. B. Paul, C. Paton, A. Norris, J. Woodhead, J. Hellstrom, J. Hergt and A. Greig, *J. Anal. At. Spectrom.*, 2012, **27**, 700-706.

26. J. Pisonero, D. Bouzas-Ramos, H. Traub, B. Cappella, C. Álvarez-Llamas, S. Richter, J. C. Mayo, J. M. Costa-Fernandez, N. Bordel and N. Jakubowski, *J. Anal. At. Spectrom.*, 2019, **34**, 655-663.
27. D. Drescher, C. Giesen, H. Traub, U. Panne, J. Kneipp and N. Jakubowski, *Anal. Chem.*, 2012, **84**, 9684-9688.
28. M. P. Mateo, G. Nicolas, V. Pinon and A. Yanez, *Surf Interface Anal*, 2006, **38**, 941-948.
29. S. M. Aberkane, M. Abdelhamid, K. Yahiaoui, C. Mahieddoune, S. Abdelli-Messaci and M. A. Harith, *Thin Solid Films*, 2018, **653**, 293-300.
30. V. Margetic, M. Bolshov, A. Stockhaus, K. Niemax and R. Hergenroder, *Journal of Analytical Atomic Spectrometry*, 2001, **16**, 616-621.
31. J. Pisonero, J. Fandino, J. H. Nordlien, S. Richter, J. Pfeifer, C. D. Quarles, J. Gonzalez, N. Jakubowski and N. Bordel, *J. Anal. At. Spectrom.*, 2019, **34**, 2252-2260.

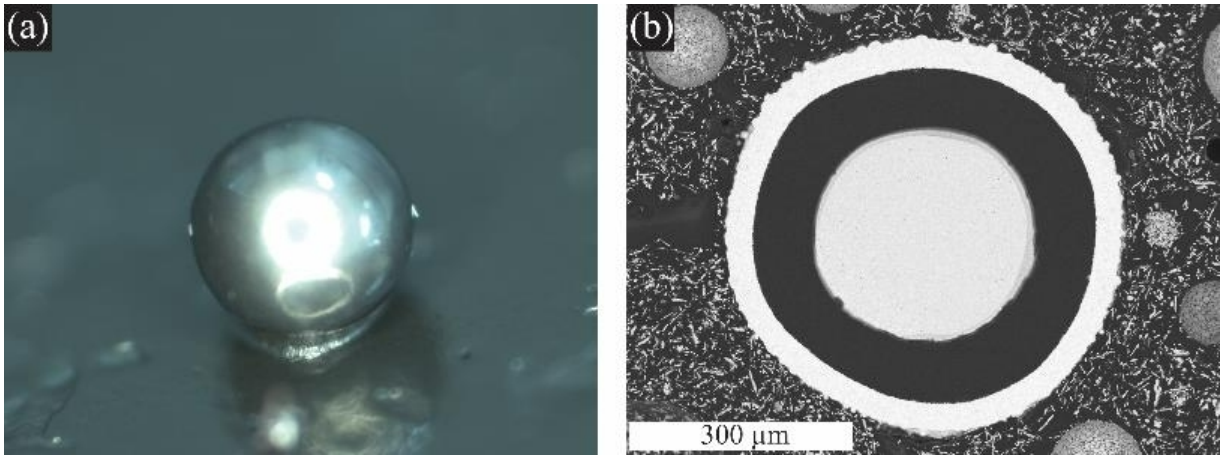

Figure 1

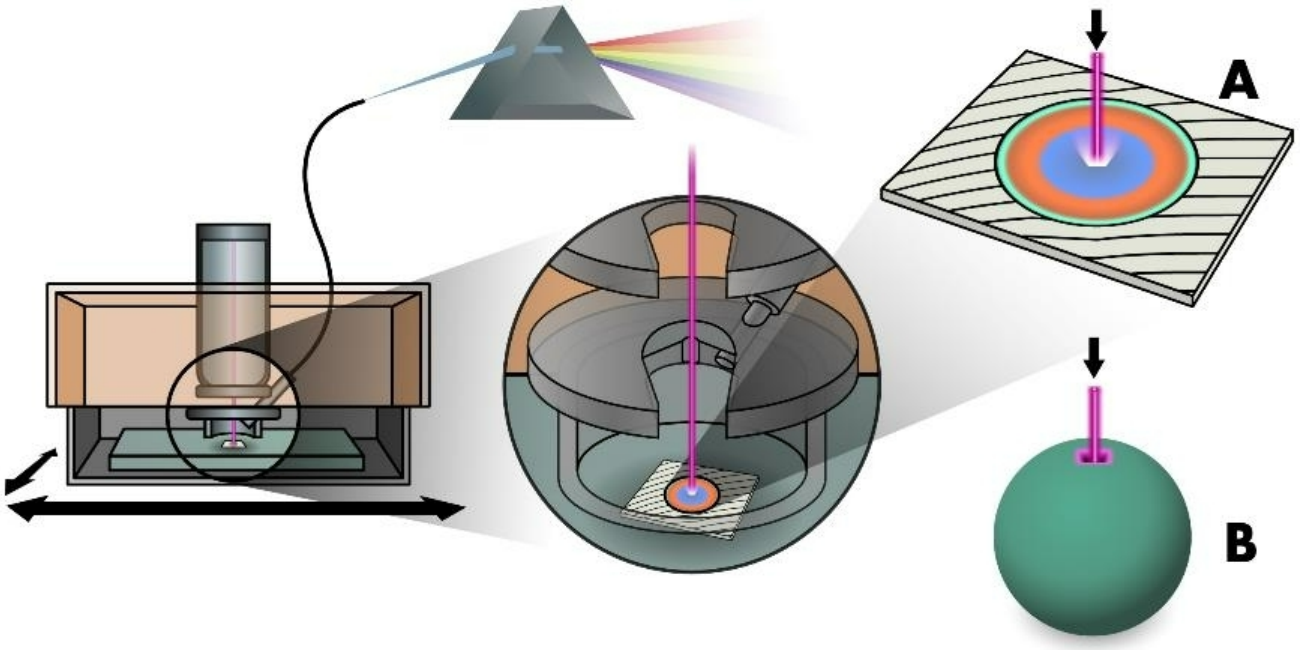

Figure 2

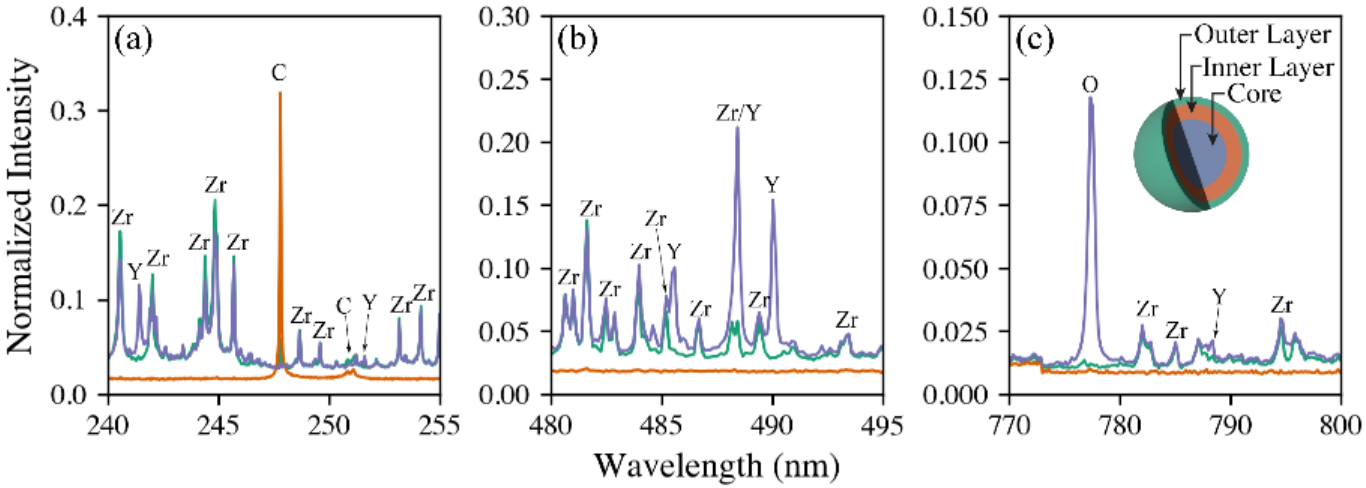
(a)
(b)
(c)
Normalized Intensity
Wavelength (nm)
Zr
Y
C
Zr/Y
O
Outer Layer
Inner Layer
Core

Figure 3

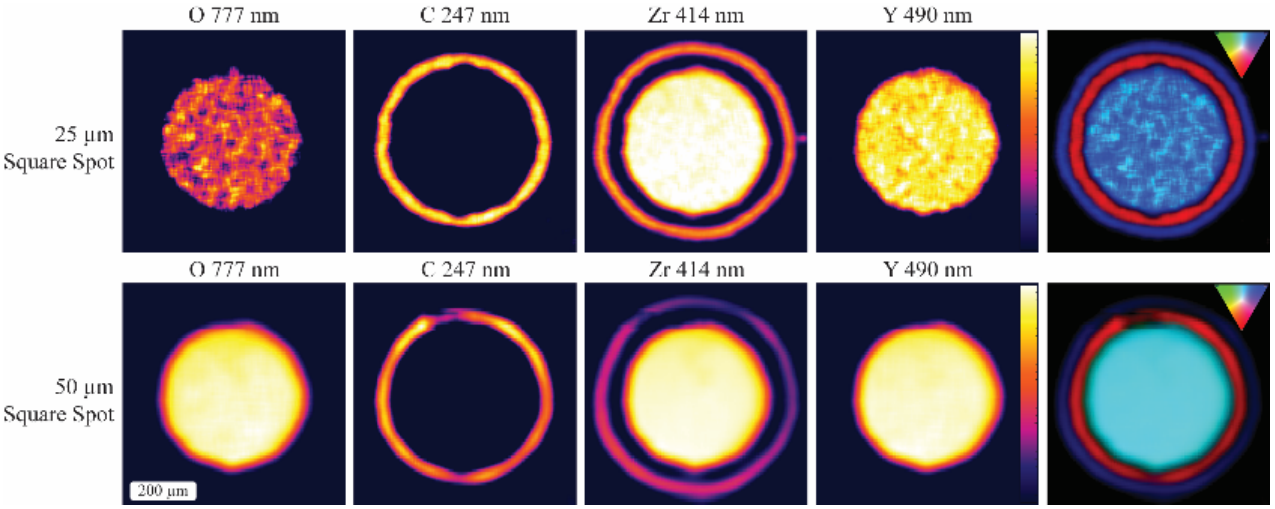
O 777 nm
C 247 nm
Zr 414 nm
Y 490 nm
25 µm
Square Spot
O 777 nm
C 247 nm
Zr 414 nm
Y 490 nm
50 µm
Square Spot
200 µm

Figure 4

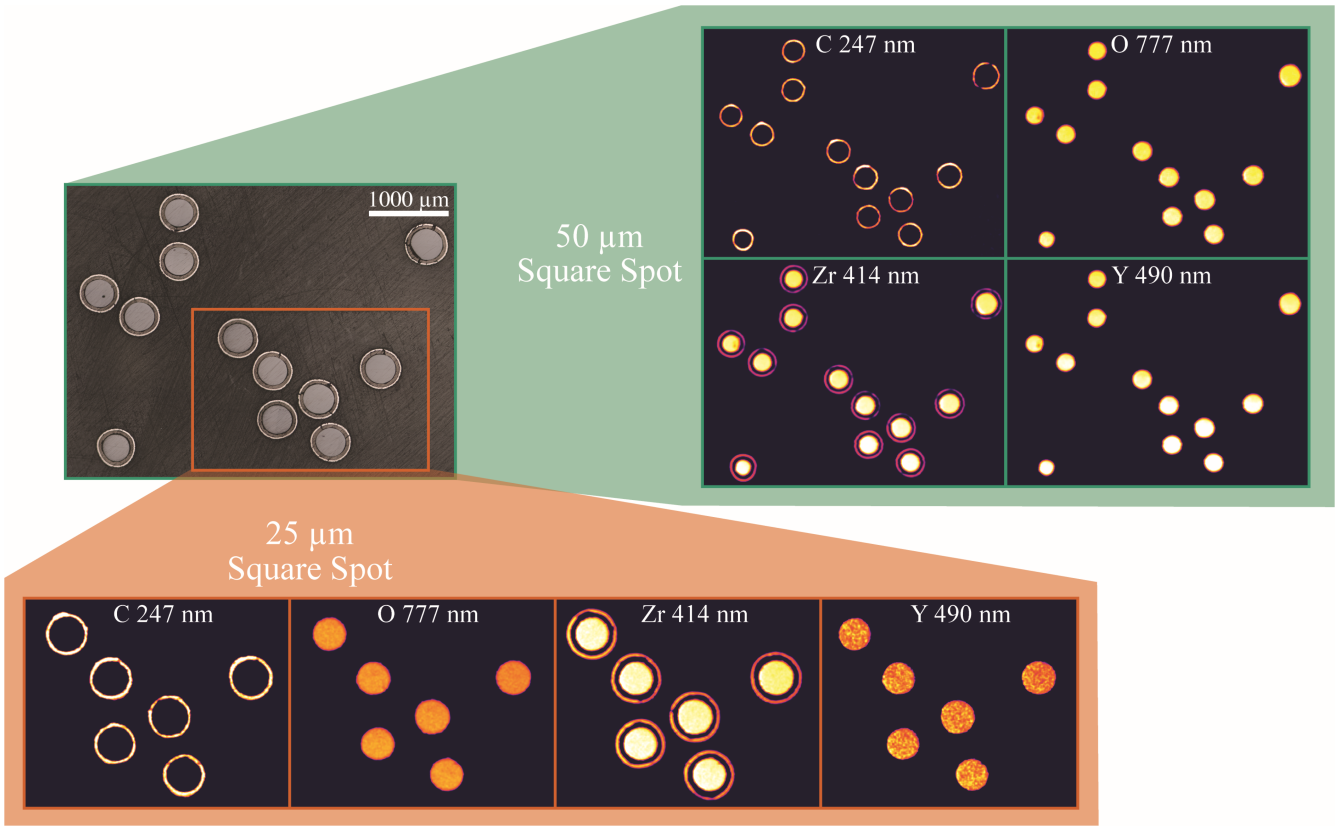
1000 µm
50 µm
Square Spot
C 247 nm
O 777 nm
Zr 414 nm
Y 490 nm
25 µm
Square Spot
C 247 nm
O 777 nm
Zr 414 nm
Y 490 nm

Figure 5

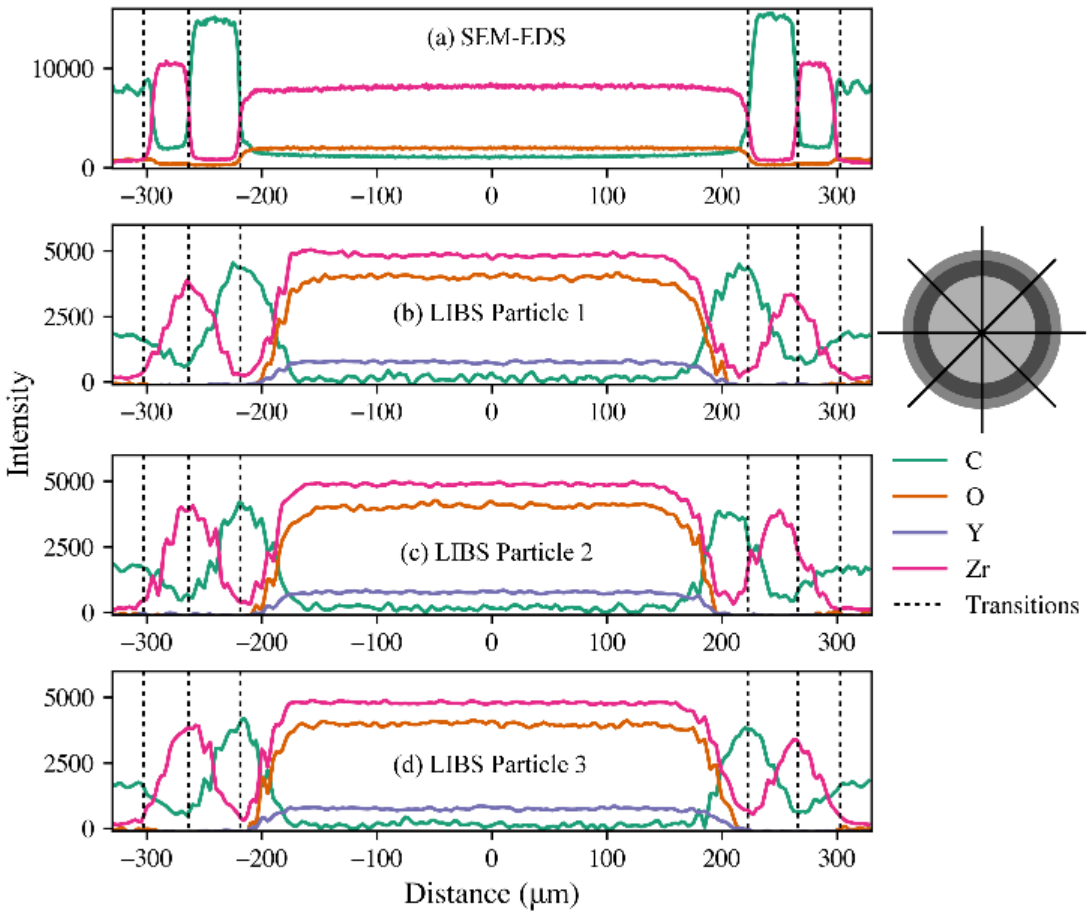
(a) SEM-EDS
(b) LIBS Particle 1
(c) LIBS Particle 2
(d) LIBS Particle 3
Intensity
Distance (μm)
C
O
Y
Zr
Transitions

Figure 6

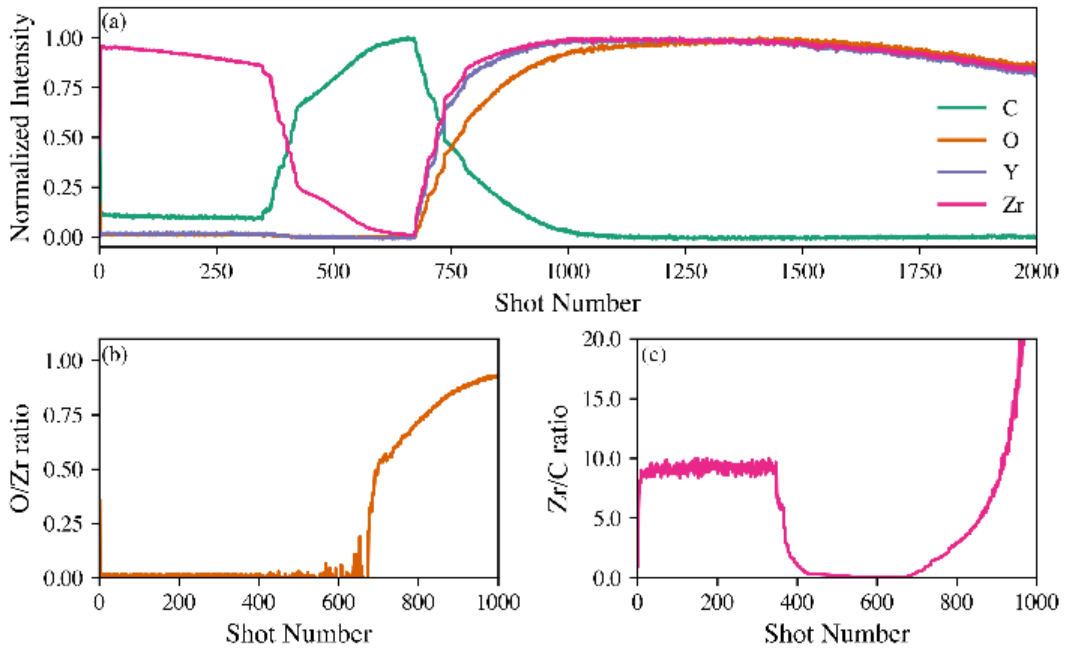
(a)
Normalized Intensity
1.00
0.75
0.50
0.25
0.00
0
250
500
750
1000
1250
1500
1750
2000
Shot Number
C
O
Y
Zr
(b)
O/Zr ratio
1.00
0.75
0.50
0.25
0.00
0
200
400
600
800
1000
Shot Number
(c)
Zr/C ratio
20.0
15.0
10.0
5.0
0.0
0
200
400
600
800
1000
Shot Number

Figure 7

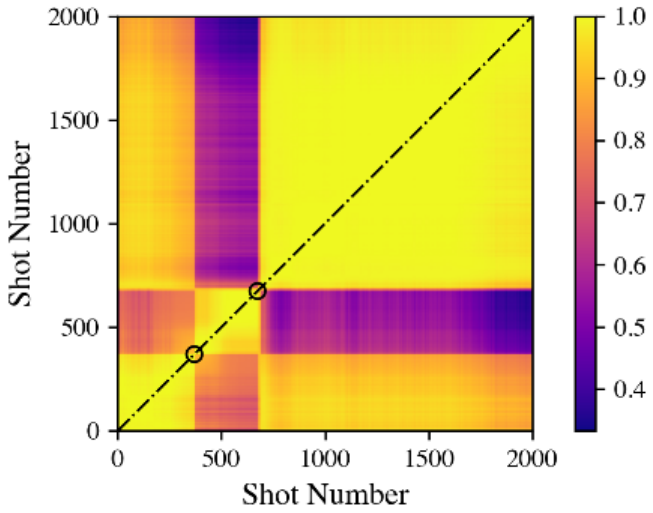
2000
1500
1000
500
0
Shot Number
0
500
1000
1500
2000
Shot Number
1.0
0.9
0.8
0.7
0.6
0.5
0.4

Figure 8